

CM² MAGAZINE



第 65 期



南方科技大学海洋磁学中心主编

<https://cm2.sustech.edu.cn/>

创刊词

海洋是生命的摇篮，是文明的纽带。地球上最早的生命诞生于海洋，海洋里的生命最终进化成了人类，人类的文化融合又通过海洋得以实现。人因海而兴。

人类对海洋的探索从未停止。从远古时代美丽的神话传说，到麦哲伦的全球航行，再到现代对大洋的科学钻探计划，海洋逐渐从人类敬畏崇拜幻想的精神寄托演变成可以开发利用与科学研究的客观存在。其中，上个世纪与太空探索同步发展的大洋科学钻探计划将人类对海洋的认知推向了崭新的纬度：深海（deep sea）与深时（deep time）。大洋钻探计划让人类知道，奔流不息的大海之下，埋藏的却是亿万年的地球历史。它们记录了地球板块的运动，从而使板块构造学说得到证实；它们记录了地球环境的演变，从而让古海洋学方兴未艾。

在探索海洋的悠久历史中，从大航海时代的导航，到大洋钻探计划中不可或缺的磁性地层学，磁学发挥了不可替代的作用。这不是偶然，因为从微观到宏观，磁性是最基本的物理属性之一，可以说，万物皆有磁性。基于课题组的学科背景和对海洋的理解，我们对海洋的探索以磁学为主要手段，海洋磁学中心因此而生。

海洋磁学中心，简称 CM²，一为其全名“Centre for Marine Magnetism”的缩写，另者恰与爱因斯坦著名的质能方程 $E = MC^2$ 对称，借以表达我们对科学巨匠的敬仰和对科学的不懈追求。

然而科学从来不是单打独斗的产物。我们以磁学为研究海洋的主攻利器，但绝不仅限于磁学。凡与磁学相关的领域均是我们关注的重点。为了跟踪反映国内外地球科学特别是与磁学有关的地球科学领域的最新研究进展，海洋磁学中心特地主办 CM² Magazine，以期与各位地球科学工作者相互交流学习、合作共进！

“海洋孕育了生命，联通了世界，促进了发展”。21 世纪是海洋科学的时代，由陆向海，让我们携手迈进中国海洋科学的黄金时代。

目 录

一、研究进展	1
1. 深海锰结核与结壳中非晶态纳米铁氧化物的古环境意义	1
二、文献速递	4
1. 日本海沟中有机碳的运输、来源和埋藏主要由突发性事件导致	4
2. 新元古代成冰纪首个地磁场强度数据及其对地球内核成核时间的可能意义	9
3. 火山内部：一个埋藏的盾状火山的三维岩浆系统结构	11
4. 永久大气氧化时间推迟 2 亿年	13
5. 南海北部中段洋陆转换带结构和破裂机制	16
6. 在最后一个冷期 Heinrich Stadial 期的干旱迫使整个地中海范围的冰川撤退	18
7. 深海环境有机质成岩作用：来自马里亚纳海沟沉积物孔隙水的地球化学启示	21
8. 反转场的角度依赖性对非磁滞剩磁应用的影响	23
9. 死海沉积物记录地磁场长期变化信息	26
10. 多指标方法揭示南大西洋西部晚更新世沉积通量和底层水环境	29

一、研究进展

1. 深海锰结核与结壳中非晶态纳米铁氧化物的古环境意义

海洋磁学中心（Centre for Marine Magnetism, CM2）团队在海洋结核与结壳的古环境研究中取得新的进展。该研究提出了一种全新的方法，可用来研究洋流活动。相关研究成果近日以“A magnetic approach to unravelling the paleoenvironmental significance of nanometer-sized Fe hydroxide in NW Pacific ferromanganese deposits”为题在地球科学期刊《地球与行星科学快报》(Earth and Planetary Science Letters)上发表。



图 1. 锰结核在深海海盆上的生长状态（深潜器海底摄像）。a-c 分别为锰结核横切面，海底摄像，单个锰结核手标本照片。

铁元素是大洋环境演变中重要元素之一，对生物地球化学循环以及碳循环具有重要意义。大洋中铁的来源主要包括粉尘、河流物质、冰碛物和海底热液。大洋海水中的铁循环主要依靠微生物作用和氧化还原环境变化调节铁的颗粒态和溶解态转变。

要想研究海洋铁循环，需要合适的载体。深海铁锰结核与结壳广泛分布于全球各个大洋，是地球表层系统中最重要铁储库。据估算，仅太平洋克拉里昂和克里伯顿区（CC 区）锰结核的铁储量就可达到 1.3×10^9 吨。这些含铁矿物相主要

为纳米级非晶态铁氢氧化物。但是，由于对纳米非晶态的特征缺乏有效的表征和定量手段，其生物地球化学循环和古环境研究中的作用被长期忽视。

海洋磁学中心研究团队创新性地使用加热方法，使样品中非晶态铁氢氧化物因受热脱水，而转变为纳米级的铁氧化物晶体（磁铁矿和赤铁矿等），提高了样品磁学响应的灵敏度，并可进一步进行高分辨率显微分析，确定其形态特征和磁学性质（图 2）。这一种新方法（加热与磁学分析）实现了对锰结核与结壳中的纳米级非晶态铁氧化物进行特征化和定量化研究。

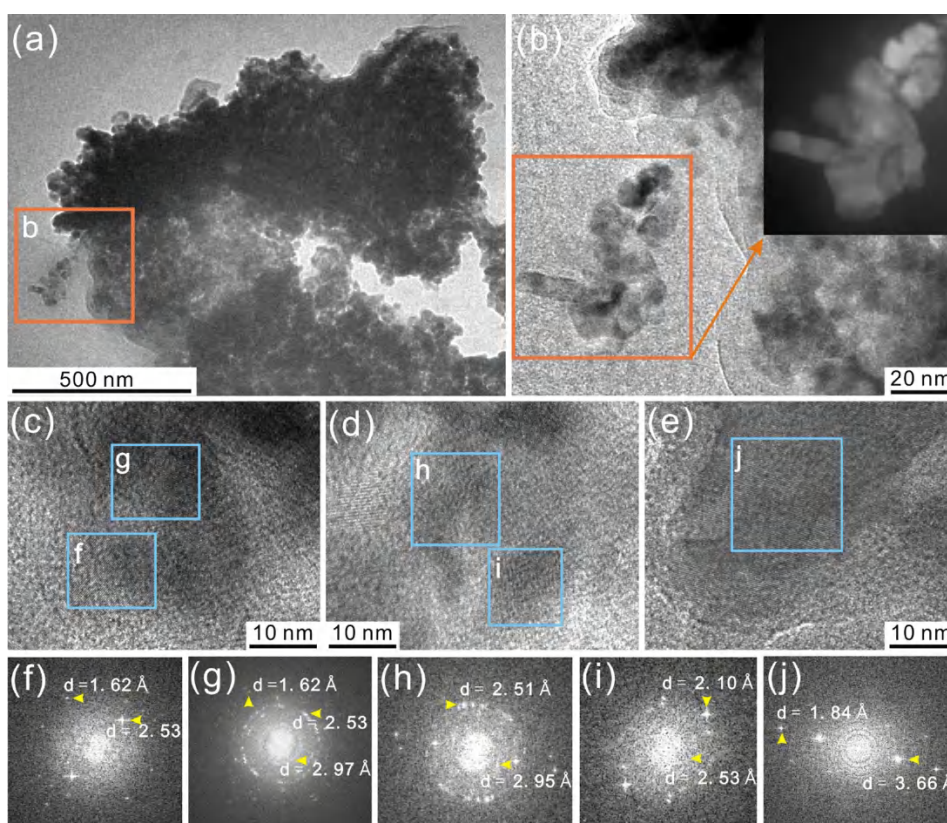


图 2. 加热 700°C 后新形成铁氧化物纳米颗粒的透射电镜分析结果。a-e 纳米矿物的形态特征。f-j 纳米矿物的花样衍射分析，这些新生成矿物主要是磁铁矿（f-g, i）以及磁赤铁矿（h）和赤铁矿（j）。

研究团队将该方法应用于西太平洋多个站位锰结核与结壳的表层样中（图 3），发现这些铁氧化物与大洋水深具有明显的对应关系，尤其是在水深 5000 米处明显增多。这一分布特点与该区海水中颗粒态铁、氧化还原敏感的微量元素、指示洋流活动的钆（Nd）同位素分布一致。该研究区 5000 米水深处具有明显的来自南极的富氧底流活动，这意味着洋流活动引起了多个环境指标响应。因此锰

结核与结壳非晶态纳米铁氧化物对洋流活动敏感，这表明研究团队提出的新方法对研究海洋古环境具有重要意义。

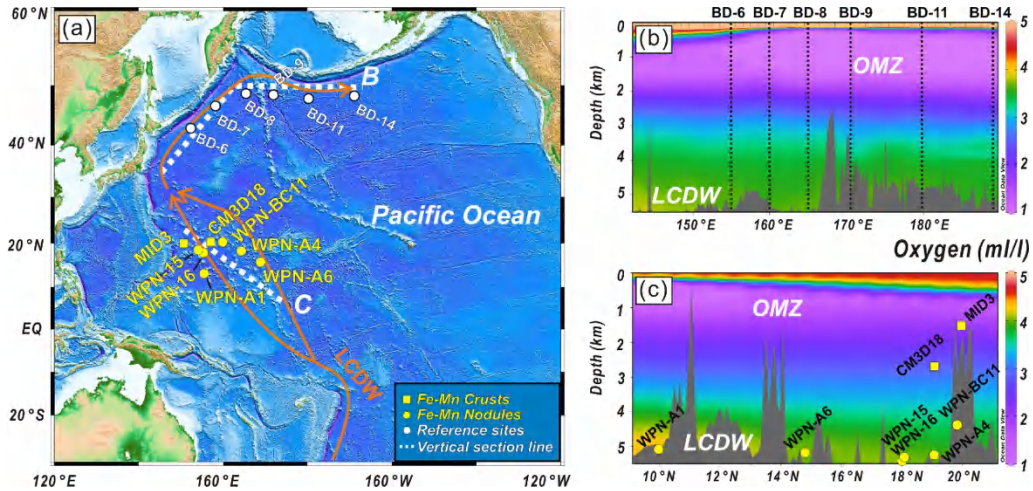


图 3. 深海锰结核与结壳以及参考点的站位分布。a 站位和参考点在西北太平洋的空间分布（Fe-Mn nodules and crusts 为铁锰结核与结壳）。b-c 站位和参考点水深分布和研究区含氧量分布（OMZ 最低含氧层，LCDW 低绕极深水流）。

南方科技大学海洋系蒋晓东研究助理教授为该论文的第一作者，周祐民助理教授和刘青松讲席教授为论文通讯作者。该研究联合澳大利亚国立大学，日本极地研究所，美国地质调查局等多个国际科研单位合作完成。以上研究得到了国家重点研发计划、国家自然科学基金、深圳市科创委与南科大启动经费的支持。

论文链接：<https://doi.org/10.1016/j.epsl.2021.116945>

Jiang, X.D., Zhao, X., Zhao, X.Y., Chou, Y.M., Hein, J.R., Sun, X.M., Zhong, Y., Ren, J.B., Liu, Q.S. (2021). A magnetic approach to unravelling the paleoenvironmental significance of nanometer-sized Fe hydroxide in NW Pacific ferromanganese deposits. *Earth and Planetary Science Letters*. 565, 116945.

作者简介：

蒋晓东 研究助理教授

研究方向为环境磁学与地球化学，主要利用岩石磁学和地球化学方法，研究深海锰结核与结壳岩石磁学性质和古环境意义。2011年获得中山大学地球科学系学士学位，留校硕博连读，于2017年获得博士学位，同年加入南方科技大学海洋磁学中心从事博士后研究，2018年赴澳大利亚国立大学从事访问学者研究工作，2020年7月聘为南方科技大学研究助理教授。目前参与和主持国家自然科学基金项目2项，省级自然科学基金项目1项，在EPSL、GRL、G-cubed、Marine Geology等学术期刊发表论文10余篇。



二、文献速递

1. 日本海沟中有机碳的输运、来源和埋藏主要由突发性事件导致

翻译人：仲义 zhongy@sustech.edu.cn



T. Schwestermann, T.I. Eglinton, N. Haghypour, et al. Event-dominated transport, provenance, and burial of organic carbon in the Japan Trench [J] Earth and Planetary Science Letters, 2021, 563, 116870.

<https://doi.org/10.1016/j.epsl.2021.116870>.

摘要：有机碳（OC）向大洋最深处的传输机制认识还不清楚，但是它可能对碳循环过程非常重要，其中包含沉积物来源与突发性事件产生的搬运过程，对最终的汇入沉积的年龄限制具有重要影响。本文中，作者综合有机质（OM）和有机碳（TOC/TN, $\delta^{13}\text{C}$, ^{14}C ）等指标，以及应用系列热氧化法（升温热解/氧化法）对跨越 2000 年沉积过程进行高分辨率记录。通过分析日本海沟南部和北部两个岩心，采集于连接陆架和海沟之间的海底峡谷系统。同时对比不存在峡谷系统的日本海沟中部地区结果。分析结果使地层记录的精确定年成为可能，并表明事件沉积物是由于海沟中部和南部区域相对表层沉积物的再活化和较深的浊流通道侵蚀以及北部区域的峡谷冲刷事件引起的。此外，研究结果表明，在半远洋海洋沉积物主要以海洋有机碳（OC），同时也与整个海沟轴上的事件沉积有关。这意味着日本海沟两侧的峡谷系统并不是陆源有机碳进入深渊地区的主要途径，热带气旋不是沉积物和碳迁移到海沟系统的主要因素。这些发现进一步支持日本海沟研究解释事件沉积来源陆地的海沟斜坡，是由地震引发的。日本海沟极低的陆源有机碳输入可以用海沟与内陆的显著距离（>180 km）来解释，不与海岸与河流系统相连的峡谷的地貌。研究认为，详细分析长期沉积记录对理解深渊海沟有机质的迁移、沉积和埋藏具有重要意义。

ABSTRACT: The delivery of organic carbon (OC) to the ocean's deepest trenches in the hadal zone is poorly understood, but may be important for the carbon cycle, contain crucial information on sediment provenance and event-related transport processes, and provide age constraints on stratigraphic sequences in this terminal sink. In this study,

we systematically characterize bulk organic matter (OM) and OC signatures (TOC/TN, $\delta^{13}\text{C}$, ^{14}C), as well as those from application of serial thermal oxidation (ramped pyrolysis/oxidation) of sediment cores recovered along an entire hadal trench encompassing high stratigraphic resolution records spanning nearly 2000 years of deposition. We analyze two cores from the southern and northern Japan Trench, where submarine canyon systems link shelf with trench. We compare results with previously published data from the central Japan Trench, where canyon systems are absent. Our analyses enable refined dating of the stratigraphic record and indicate that event deposits arise from remobilization of relatively surficial sediment coupled with deeper erosion along turbidity current pathways in the southern and central study site and from canyon flushing events in the northern study site. Furthermore, our findings indicate deposition of predominantly marine OC within hemipelagic background sediment as well as associated with event deposits along the entire trench axis. This implies that canyon systems flanking the Japan Trench do not serve as a short-circuit for injection of terrestrial OC to the hadal zone, and that tropical cyclones are not major agents for sediment and carbon transfer into this trench system. These findings further support previous Japan Trench studies interpreting that event deposits originate from the landward trench slope and are earthquake-triggered. The very low terrestrial OC input into the Japan Trench can be explained by the significant distance between trench and hinterland (>180 km), and the physiography of the canyons that do not connect to coast and river systems. We suggest that detailed analyzes of long sedimentary records are essential to understand OC transfer, deposition and burial in hadal trenches.

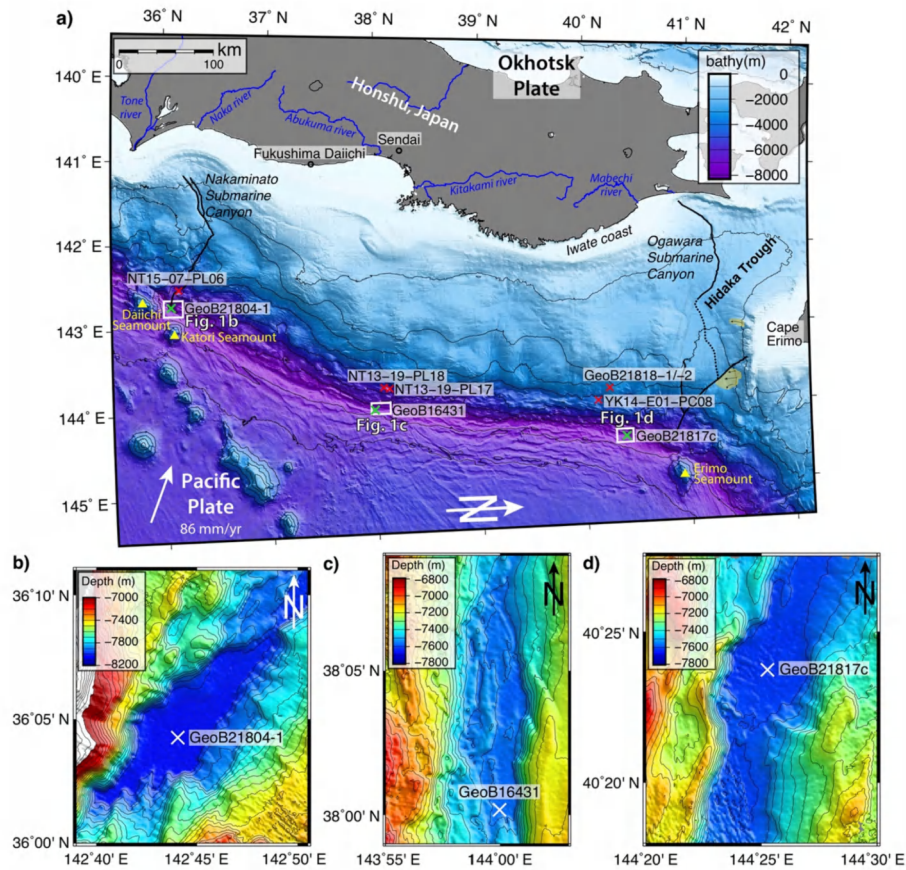


Fig1. a) Bathymetric overview map of the Japan Trench (Strasser et al., 2017; Kioka et al., 2019a) between the Daiichi Seamount in the South and the Erimo Seamount in the North with 1000-m contour lines. Red crosses mark core locations on the slope, whereas green crosses mark core locations in the trench. Black bold lines mark the Nakaminato and Ogawara canyon in the South and North, respectively. Yellow shaded areas off Cape Erimo indicate scarps of submarine landslides of unknown age. (note clockwise-rotation of the map by 90 degrees) b) Bathymetric map of the southern basin with 50-m contour lines and core location GeoB21804-1; c) Bathymetric map of the central basin with 50-m contour lines and core location GeoB16431; d) Bathymetric map of the northern basin with 50-m contour lines and core location GeoB21817c. (For interpretation of the colors in the figure(s), the reader is referred to the web version of this article.)

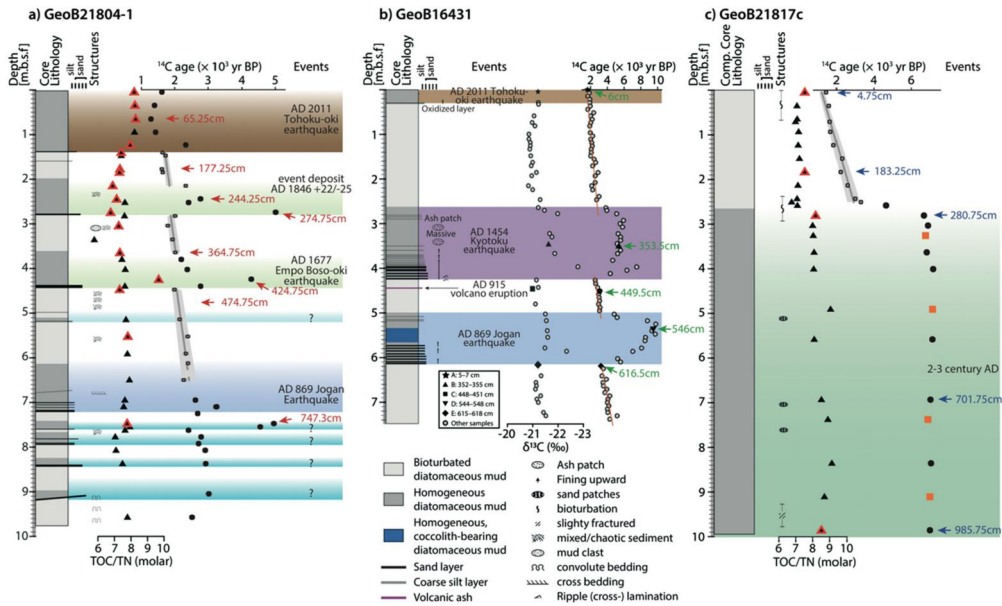


Fig2. a) Core GeoB21804-1 collected in the southern basin with litholog (after Strasser et al., 2017), TOC/TN (triangles), bulk OC ^{14}C ages (circles), and interpretation of event deposits (after Kioka et al., 2019b). b) Reference core Geob16431 from the central basin with litholog (Ikehara et al., 2016), bulk OC $\delta^{13}\text{C}$ values and bulk OC ^{14}C ages (data of Bao et al. (2018b)). c) Core GeoB21817c retrieved in the northern basin with litholog (after Strasser et al., 2017), TOC/TN, and bulk OC ^{14}C ages. Triangles with red border in a) and c) were further analyzed for $\delta^{13}\text{C}$. Bulk OC ^{14}C ages within the background sediment in a) and c) are after Kioka et al. (2019b). Four bulk OC ^{14}C ages marked with orange rectangles are after Usami et al. (2021). Samples marked with red (a), green (b), and blue (c) arrows were further processed on the RPO (samples in (b) by Bao et al., 2018b).

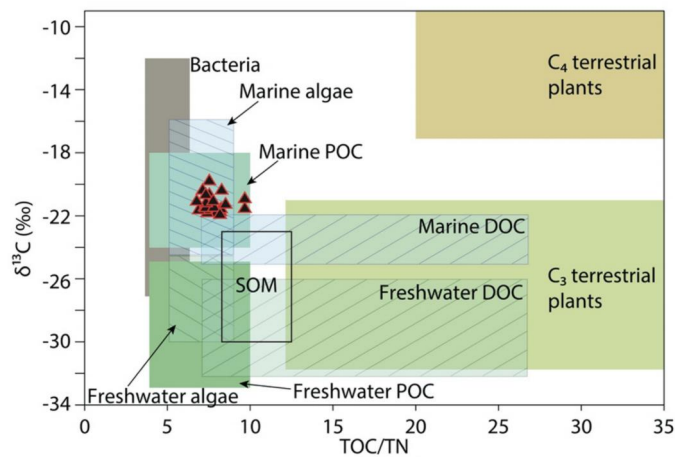


Fig3. Diagram (modified after Goni et al., 2008 and Lamb et al., 2006, and references therein) indicating the provenance of the samples based on TOC/TN and $\delta^{13}\text{C}$, indicating marine origin (POC = particulate organic carbon, SOM = soil organic matter, DOC = dissolved organic matter). Triangles indicate Japan Trench sediments.

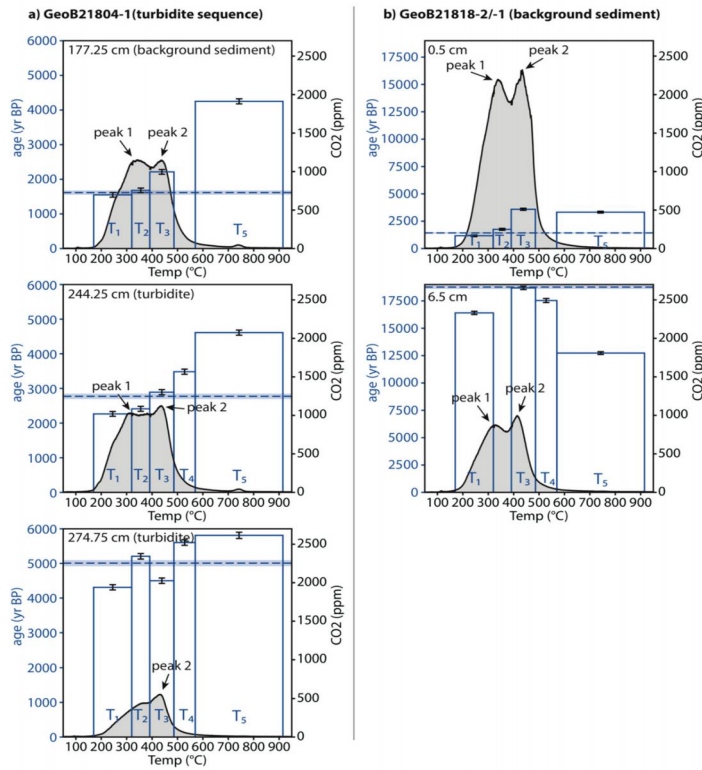


Fig4. a) Sequence from background sediment (177.25 cm) to turbidite (244.75 cm and 274.75 cm) of core GeoB21804-1 present an age increase in all 5 temperature fractions (T1–T5), indicating remobilization of slightly older carbon. The thermograms show an overall decrease in TOC content towards the base of the turbidite, especially of peak 1, which disappears in sample 274.75 cm. b) Thermograms of hemipelagic background sediments of the slope core GeoB21818-2/-1 present decreased TOC content within older sediment, while peak 1 and 2 remain similar.

2. 新元古代成冰纪首个地磁场强度数据及其对地球内核成核时间的可能意义

翻译人：柳加波 liujb@sustech.edu.cn



Lloyd S J, Biggin A J, Halls H, et al. *First palaeointensity data from the cryogenian and their potential implications for inner core nucleation age[J]. Geophysical Journal International, 2021, 226(1): 66-77.*

<https://doi.org/10.1093/gji/ggab090>

摘要：地球内核的成核时间是地球演化历史中及其重要的事件，这也是一直争论的焦点。最新的一些理论估计认为，成核年龄可能在新元古代期间的任何时候。这比人们以前认知的成核时间要晚很多。年轻的地球内核需要比现今地核更快的冷却速率以及一个可能比之前地核更高的温度。了解内核的形成年代对研究地球的热量变化以及总的能量收支具有重要意义。使用地球发电机数值模型的预测需要针对这些数据进行测试。但是现有的记录太过稀疏，很难将内核的形成年代限制在一个精确的时间段内。本文，我们报道了 720 百万年前来自富兰克林大火成岩省（Franklin Large Igneous Province）的白云母岩脉（以及一个基岩）的研究结果。这些样品填补了非常关键的约 300 个百万年的古强度记录空白。这项研究对分布在加拿大北极地区和格陵兰岛的 11 个站点的整个岩石样品使用了三种独立的技术。最终获得了 5 至 11 ZAm² 的虚拟地磁偶极子场强度（VDM），平均强度为 11 ZAm²，这比现今地磁场强度几乎低了一个量级。这些非常弱的地磁场强度和最近报道的埃迪卡拉纪（比本文晚近 150 百万年）的非常弱的地磁场强度相吻合。这可能支持在年轻的内核形成之前，地球发电机在新元古代已经处于崩溃的边缘。

ABSTRACT: The timing of inner core nucleation is a hugely significant event in Earth's evolution and has been the subject of intense debate. Some of the most recent theoretical estimates for the age of nucleation fall throughout the Neoproterozoic era; much younger than previously thought. A young inner core requires faster recent core cooling rates and a likely hotter early core; knowledge of its age would be invaluable in understanding Earth's thermal history and total energy budget. Predictions generated

by numerical dynamo models need to be tested against such data, but records are currently much too sparse to constrain the event to a precise period of time. Here, we present results from 720 Ma dolerite dykes (and one sill) from the Franklin Large Igneous Province, which fall within a crucial 300 Myr gap in palaeointensity records. This study uses three independent techniques on whole rocks from 11 sites spread across High Arctic Canada and Greenland to produce virtual dipole moments ranging from 5 to 20 ZAm^2 (mean 11 ZAm^2); almost one order of magnitude lower than the present-day field. These weak-field results agree with recent ultralow palaeointensity data obtained from Ediacaran rocks formed ~ 150 Myr later and may support that the dynamo was on the brink of collapse in the Neoproterozoic prior to a young inner core formation date.

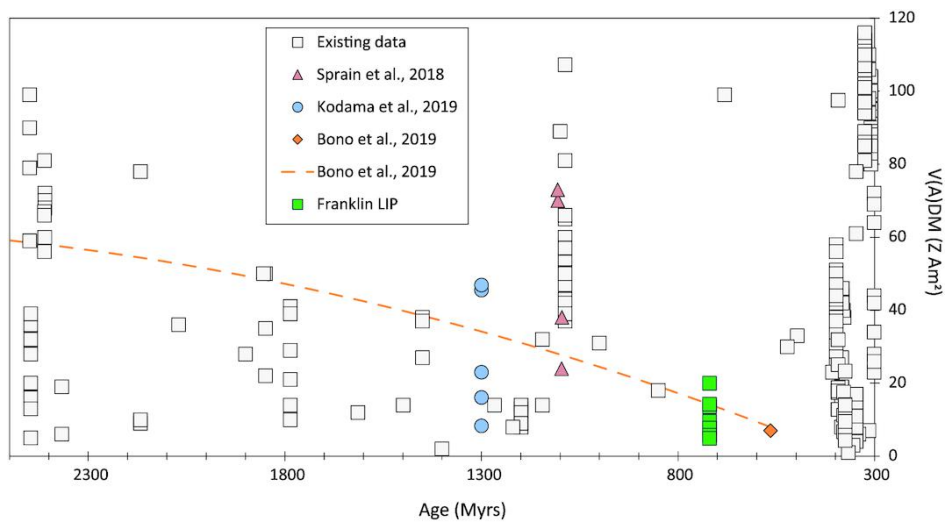


Fig 1. Virtual (axial) dipole moment data (V(A)DM) through time (300 – 2500 Ma). Data taken from the PINT database (v.2015.05; <http://earth.liv.ac.uk/pint/>; Biggin *et al.* 2015) with the addition of recent data from Shcherbakova *et al.* 2017, Sprain *et al.* 2018, Hawkins *et al.* 2019, Kodama *et al.* 2019 and Bono *et al.* 2019. The dashed line is the weighted second-order polynomial regression of Precambrian field strength data by Bono *et al.* 2019. Data >500 Myr has been filtered to exclude VDM data with $Q_{PI} < 3$, $N < 3$.

3. 火山内部：一个埋藏的盾状火山的三维岩浆系统结构

翻译人：冯婉仪 fengwy@sustech.edu.cn



Walker F, Schofield N, Millett J, et al. *Inside the volcano: Three-dimensional magmatic architecture of a buried shield volcano*[J]. *Geology*, 2021, 49, 243-247.

<https://doi.org/10.1130/G47941.1>

摘要：岩浆通道系统的性质与形成对火成地质学十分重要。传统上，岩浆房被认为是快速侵位的熔岩体或部分结晶的“岩浆晶粥”，并且通过一个狭窄的圆柱形管道连接至地表（被称为“气球和吸管”模型）。然而，最近的数据表明，火山之下的岩浆房是通过较小的侵入体合并而逐渐形成的。在这里，我们展示了第一个高分辨率的三维重建的古老火山通道系统，该系统包含一个大型的岩盖式复合体。通过对地震反射和重力资料的综合分析，我们认为~200km³的岩盖是由较小的侵入体局部合并而成。这个复合体似乎既促进了地表的火山活动，也助长了火山机构之下广泛的岩床网络。大量岩床在火山通道内被成像，表明岩浆在其上升过程中在地壳不同深度停留。我们的研究结果首次揭示了一个大型古盾状火山之下的整个多组分通道系统。

ABSTRACT: The nature and growth of magmatic plumbing systems are of fundamental importance to igneous geology. Traditionally, magma chambers have been viewed as rapidly emplaced bodies of molten rock or partially crystallized “magma mush” connected to the surface by a narrow cylindrical conduit (referred to as the “balloon-and-straw” model). Recent data suggest, however, that magma chambers beneath volcanoes are formed incrementally through amalgamation of smaller intrusions. Here we present the first high-resolution three dimensional reconstruction of an ancient volcanic plumbing system as a large laccolithic complex. By integrating seismic reflection and gravity data, we show that the ~ 200 km³ laccolith appears to have formed through partial amalgamation of smaller intrusions. The complex appears to have fed both surface volcanism and an extensive sill network beneath the volcanic edifice. Numerous sills are imaged within the volcanic conduit, indicating that magma

stalled at various levels during its ascent. Our results reveal for the first time the entire multicomponent plumbing system within a large ancient shield volcano.

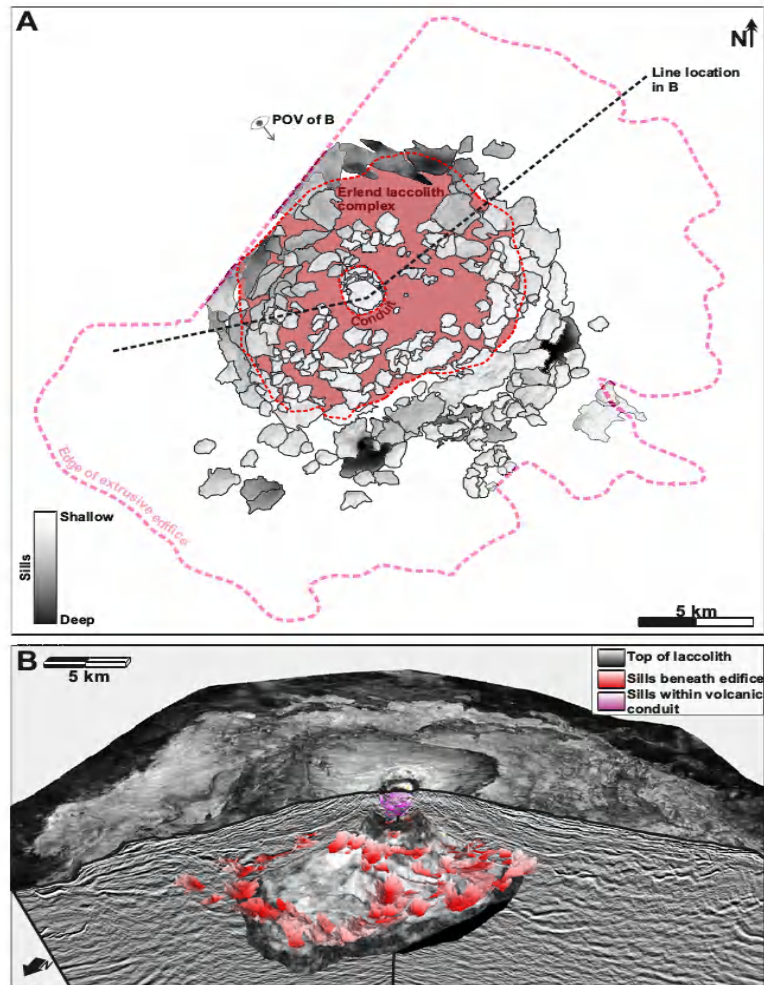


Fig1. (A) Top-down view of Erlend volcano (Faroe-Shetland Basin) plumbing system, showing all sill intrusions mapped from 3-D seismic reflection data, plus edifice edge, laccolith and conduit. Sills are radially distributed around the conduit and laccolith. POV—point of view. (B) Oblique three dimensional (3-D) view of Erlend volcano created from 3-D seismic reflection data, showing seismic line combined with the top surface of the edifice to the southeast and plumbing system to the northwest. Tops of the edifice and laccolithic complex are displayed using root mean square (RMS) amplitude to improve contrast with colored sills. Red sills are beneath the edifice, many connected to the top of the laccolith. Purple sills are within the conduit. For a complete 3-D view of the plumbing system, see Figure S3 (see footnote 1)

4. 永久大气氧化时间推迟 2 亿年

翻译人：张琪 zhangq7@sustech.edu.cn



Poulton S W, Bekker A, Cumming V M, et al. A 200-million-year delay in permanent atmospheric oxygenation [J]. Nature, 2021, 592, 232-236.

<https://doi.org/10.1038/s41586-021-03393-7>

摘要：大气中氧气的增加从根本上改变了表层环境化学和地球的宜居性。早期的大气氧化事件发生在以多次全球冰川作用为标志的漫长极端气候不稳定时期，氧气浓度最初上升到目前大气水平的 10^{-5} 以上的时间约为 24.3 亿年前。随后大气氧含量的波动被认为发生在约 23.2 亿年前，这也被认为代表了大气不可逆氧化的大概时间。我们报告一个来自南非的特兰斯瓦尔超群的海洋沉积物记录的高分辨率跨越早古生代最后两次冰期的大气和区域海洋氧化还原环境的重建。利用多种硫同位素和铁-硫-碳系统分类，我们证明了大约 23.2 亿年前之后大气中氧含量的持续振荡与海洋氧化还原化学和气候的重大扰动有关。因此，氧气水平在目前大气水平的 10^{-5} 的阈值上波动了约 2 亿年，随着 Lomagundi 碳同位素漂移事件在约 22.2 亿年前最终实现了大气永久氧化，比目前估计的时间晚了约 1 亿年。

ABSTRACT: The rise of atmospheric oxygen fundamentally changed the chemistry of surficial environments and the nature of Earth's habitability. Early atmospheric oxygenation occurred over a protracted period of extreme climatic instability marked by multiple global glaciations, with the initial rise of oxygen concentration to above 10^{-5} of the present atmospheric level constrained to about 2.43 billion years ago. Subsequent fluctuations in atmospheric oxygen levels have, however, been reported to have occurred until about 2.32 billion years ago, which represents the estimated timing of irreversible oxygenation of the atmosphere. Here we report a high-resolution reconstruction of atmospheric and local oceanic redox conditions across the final two glaciations of the early Palaeoproterozoic era, as documented by marine sediments from the Transvaal Supergroup, South Africa. Using multiple sulfur isotope and iron-sulfur-carbon systematics, we demonstrate continued oscillations in atmospheric oxygen

levels after about 2.32 billion years ago that are linked to major perturbations in ocean redox chemistry and climate. Oxygen levels thus fluctuated across the threshold of 10^{-5} of the present atmospheric level for about 200 million years, with permanent atmospheric oxygenation finally arriving with the Lomagundi carbon isotope excursion at about 2.22 billion years ago, some 100 million years later than currently estimated.

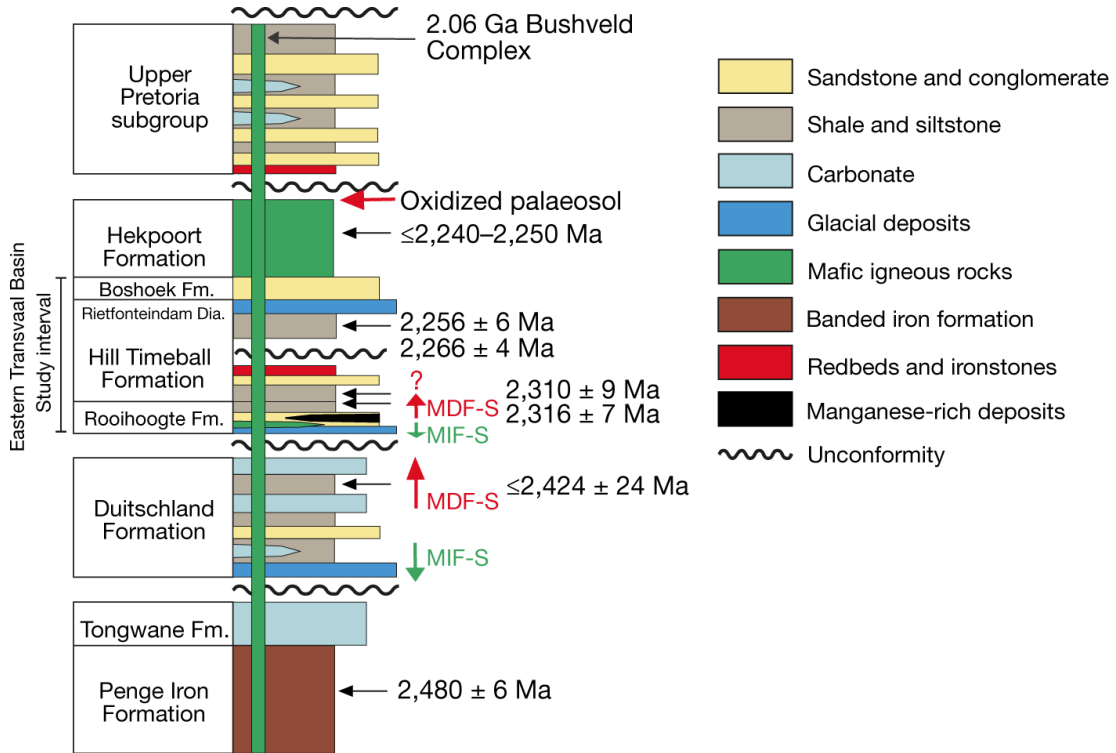


Fig1. Simplified Palaeoproterozoic stratigraphy of the Eastern Transvaal Basin, South Africa, showing the studied interval.

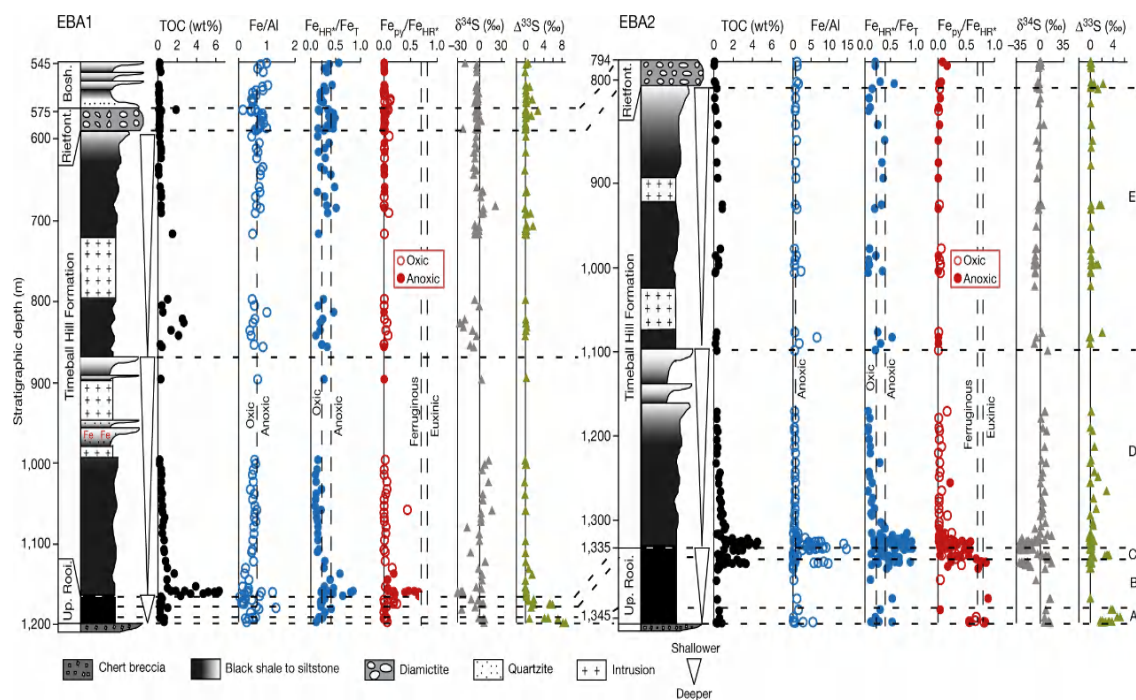


Fig2. Geochemical and isotopic profiles for drill cores EBA-1 and EBA-2. For clarity, the stratigraphic depth scale for Rietfontein Diamictite (Rietfont.) and Boshhoek Formation (Bosh.) in drill core EBA-1 and for Rietfontein Diamictite and Rooihogte Formation (Up. Rooi.) in drill core EBA-2. The dashed line on the Fe/Al plots represents the boundary (0.66) for distinguishing oxic and anoxic water-column conditions. The dashed lines on the FeHR*/FeT plots represent the boundaries for distinguishing oxic (<0.22) and anoxic (>0.38) water-column conditions³⁸. The dashed lines on the Fe_{py}/Fe_{HR*} plots represent the boundaries for distinguishing euxinic (>0.8) and ferruginous (<0.7) water-column conditions, which are applicable only to samples deposited from an anoxic water column (closed circles). Fe_{HR*}/Fe_T and Fe_{py}/Fe_{HR*} ratios are corrected for transformation of unsulfidized FeHR to Fe-rich clays during diagenesis (see Methods). Horizontal dashed lines divide the succession into informal intervals (A–E) to aid interpretational clarity.

5. 南海北部中段洋陆转换带结构和破裂机制

翻译人: 刘伟 inewway@163.com



Zhang C, Sun Z, Manatschal G, et al. *Ocean-continent transition architecture and breakup mechanism at the mid-northern South China Sea*[J]. *Earth-Science Reviews*, 2021(3):103620.

<https://doi.org/10.1016/j.earscirev.2021.103620>

摘要: 洋陆转换带(OCT)位于大陆和海洋地壳之间, 是了解板块构造最基本过程的天然实验室, 有助于理解新的板块边界的形成机制, 也就是岩石圈破裂过程。然而, OCT 的位置和结构以及控制大陆岩石圈破裂和新洋壳形成的过程仍存在争议。本文利用最新的高分辨率地震反射剖面显示的南海北部明显的陆壳到洋壳的完整过渡带, 并结合 IODP 钻孔和重力数据, 定位了 OCT 的位置, 并研究了岩石圈发生破裂的时间、地点和方式。根据地震反射资料的观测和解释, 确定了南海 OCT 的界线。结果表明, OCT 基底对应的是拆离减薄地壳和同构造期火成岩物质侵位造成的混合地壳。南海北部岩石圈和其共轭边缘的破裂是不对称的, 表现为复合结构, 这与朝海方向板块分离过程逐渐由构造控制转变为岩浆控制有关。此外, 观测结果还表明, 在 30 公里的横向距离上存在一个从下板块裂陷边缘向上板块裂陷边缘的沿走向的转变。基底结构的强烈变异性和拆离状态的转变指示了一个转换带, 其可以解释大陆边缘的分段性。这种分段可能是由于继承性的前裂谷期地壳或岩石圈非均质性造成的。值得注意的是, 分段并没有控制大陆破裂和随后的海洋增生。

ABSTRACT: Ocean-Continent Transition (OCT) located between the edge of the continental and unequivocal oceanic crusts is an ideal laboratory to understand one of the most fundamental processes of Plate Tectonics, namely the formation mechanism of a new plate boundary, also referred to as lithospheric breakup. However, the location and architecture of the OCT and the processes governing the rupture of continental lithosphere and creation of new oceanic crust remain debated. In this paper, we present newly released high-resolution seismic reflection profiles that image the complete

transition from unambiguous continental to oceanic crusts in the mid-northern South China Sea (SCS), accompanied with IODP drill holes and gravity data, with the aim to map the OCT and explore where, when and how lithospheric breakup occurred. Based on observations and interpretations of seismic reflection data, we define the limits of the SCS OCT. The results show that the OCT basement corresponds to hybrid crust resulting from the complex interaction between crustal thinning along detachment systems and emplacement of new syn-tectonic igneous materials. The lithospheric breakup in the northern SCS and the conjugate margin occurred asymmetrically and was accomplished by core-complex type structures related to an oceanward transition from tectonic to magma-controlled processes during plate separation. Additionally, the observations suggest a sharp along-strike transition from a lower to an upper plate rifted margin setting over a lateral distance of 30 km. The strong variability in the basement architecture and the abrupt flip in detachment polarity imply a transfer zone to explain the segmentation of the margin. Such segmentation may result from inherited pre-rift crustal and/or lithospheric heterogeneities. Notably, the segmentation did not control breakup and subsequent oceanic accretion.

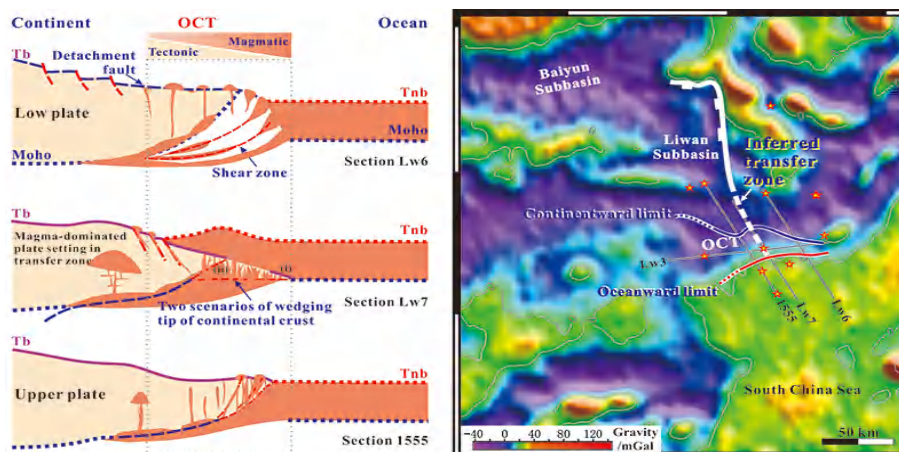


Fig1. Along-strike abrupt flip of the detachment polarity suggests a transition from lower-plate to upper-plate rifted margin setting in the ocean-continent transition (OCT), and the breakup was accomplished by core-complex type structures in the northern SCS. The variation of the basement architecture and detachment polarity in the OCT implies a transfer zone accounting for the segmentation of the margin.

6. 在最后一个冷期，Heinrich Stadial 期的干旱迫使整个地中海范围的冰川撤退

翻译人：王浩森 11930841@mail.sustech.edu.cn



Allard J L, Hughes P D, Woodward J C. *Heinrich Stadial aridity forced Mediterranean-wide glacier retreat in the last cold stage*[J]. *Nature Geoscience*, 2021: 1-9.

<https://doi.org/10.1038/s41561-021-00703-6>

摘要： 在最后一个冰期的整个阶段，北大西洋地区气候环境因突然的气候变化而中断，并且大气过程将其影响传播到了邻近的大陆。在 Heinrich Stadials 期间，大片冰原上脱落的冰山使海洋变冷。不同温度和降水指标的变化对晚更新世高山冰川和陆地发育的影响知之甚少。我们利用地中海三大洲的冰川陆地分析了 1,118 个宇宙成因暴露年龄（跨越了 100,000 年）。根据地貌背景，并按沉积环境和地理区域对记录进行分层。该数据库包括 300 个冰碛点。尽管温度较低，但 Heinrich Stadial 干旱仍造成了冰川减少，并在整个地中海地区阻碍了冰川的增长。相反，Heinrich Stadials 之间相对温暖和潮湿的气候有利于冰川的积累，从而导致整个地区的冰川生长和冰碛形成。我们的结论为最后一个寒冷阶段地中海盆地 Heinrich Stadial 干旱的反复和广泛分布的气候模式模型提供了支持。Heinrich Stadials 期也同样看到了山谷两侧的粗碎屑的增加。这些气候变化的累积造成地貌影响在冰川周期的顶点达到了最大的冰碛形态。

ABSTRACT: Throughout the last cold stage, the North Atlantic region was punctuated by abrupt climate shifts and atmospheric processes propagated their effects to adjacent continents. During Heinrich Stadials, the ocean was chilled by icebergs calved from the great ice sheets. The impact of multiple temperature and precipitation regime changes on Late Pleistocene mountain glaciers and landscape development is poorly understood. Here we analyse 1,118 cosmogenic exposure ages—spanning the last 100,000 years—from glacial landforms on three continents across the Mediterranean. We evaluate their geomorphological context and stratify the record by depositional setting and

geographical region. The database includes 300 dated moraines. We show that, despite cold temperatures, Heinrich Stadial aridity caused negative glacier mass balance and repeatedly stalled glacier growth across the Mediterranean. In contrast, relatively warm and humid climates between Heinrich Stadials favoured positive glacier mass balance, resulting in region-wide glacier growth and moraine formation. Our analysis supports climate model simulations of repeated and widespread Heinrich Stadial aridity in the Mediterranean basin during the last cold stage. Heinrich Stadials also saw enhanced supply of coarse debris from valley sides. The cumulative geomorphological impact of these climate shifts saw the largest moraines form at the culmination of the glacial cycle.

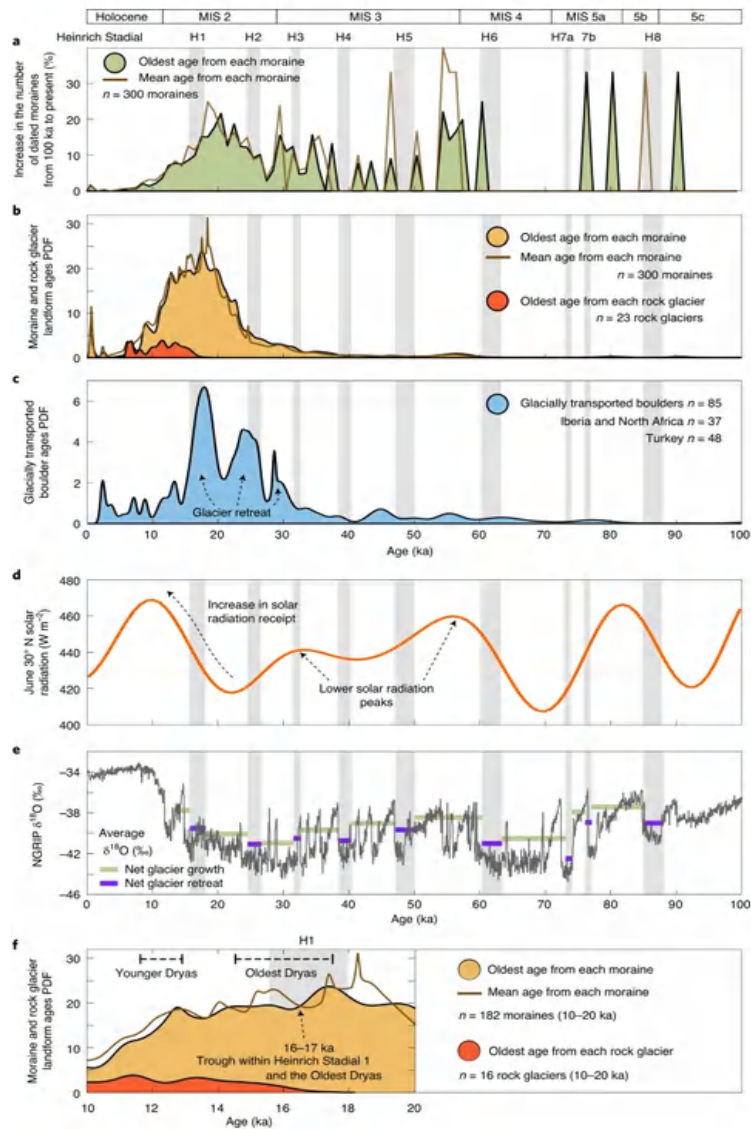


Fig1. a, Percentage increase in the number of dated moraines from 100 ka to present plotted at 1,000 yr resolution. The two oldest peaks are capped at 33% for plotting purposes. The data here are compiled from published sources in the database. b, Probability density function (PDF) of moraine landform and rock glacier landform ages. c, PDF of ages from glacially transported boulders. d, June solar radiation at 30° N. e, The North Greenland Ice Core Project (NGRIP) $\delta^{18}\text{O}$ (‰) record (purple and green lines show mean $\delta^{18}\text{O}$ (‰) values within and between Heinrich Stadials, respectively, to represent average climate conditions within these periods). f, PDF of moraine and rock glacier ages through Termination 1 and the Late-glacial (10–20 ka). The chronology for Heinrich Stadials is based on published sources

7. 深海环境有机质成岩作用:来自马里亚纳海沟沉积物孔隙水的地球化学启示

翻译人: 王敦繁 dunfan_w@foxmail.com



Liu S, Peng X. *Organic matter diagenesis in hadal setting: Insights from the pore-water geochemistry of the Mariana Trench sediments*[J]. *Deep Sea Research Part I Oceanographic Research Papers*, 2019, 147(MAY):22-31.

[https://doi: 10.1016/j.dsr.2019.03.011](https://doi.org/10.1016/j.dsr.2019.03.011)

摘要: 深海沉积环境(> ~ 6000 m 水深)中有机质的成岩作用研究较少。在这项研究中, 我们通过对马里亚纳海沟深渊(5500-10257 m)沉积物的孔隙水地球化学测量, 计算通量和成岩速率计算, 量化有机质的氧化过程。底栖生物总氧耗量、硝化反硝化深度综合速率与水深呈正相关关系, 表明有机质成岩作用在深渊带深部有所增强。水深与氧/硝酸盐渗透深度的负线性关系进一步支持了这一结论。在深水区, 有机质降解主要是有氧呼吸作用, 厌氧作用可以忽略不计。反硝化作用在厌氧有机质降解过程中起着重要作用, 约占深渊综合有机质矿化总量的 5%。此外, 我们的研究结果表明, 硝化和反硝化之间存在着显著的直接耦合关系, 这可能决定了氮的转换。虽然并非没有不确定性, 但我们的研究结果揭示了地球海洋最深处沉积成岩作用中反硝化作用的重要性, 并可能对了解深渊带生物地球化学循环的当前状态具有重要意义。

ABSTRACT: The diagenetic processes of organic matter (OM) in hadal sedimentary environments (> 6000 m water depth) are much less studied than those in other accessible environments. In this study, we quantify OM oxidation processes using pore-water geochemical measurements, fluxes, and diagenetic rate calculations in sediments along a depth transect from abyssal to hadal sites (5500–10257 m) in the Mariana Trench. The total benthic O₂ consumption, and depth-integrated rates of nitrification and denitrification are positively correlated with water depth, indicating that OM diagenesis is enhanced in the deep sites of the hadal zone. The negative linear correlation between water depth and oxygen/nitrate penetration depths further supports this conclusion. In the abyssal sites, aerobic respiration dominates OM degradation, and

anaerobic processes are negligible. In contrast, denitrification plays an important role in anaerobic OM degradation, and accounts for approximately 5% of the depth-integrated total OM mineralization at the deepest hadal site. Moreover, our results suggest that direct coupling between nitrification and denitrification is significant, and may define the turnover of N in hadal sediments. Although they are not without uncertainties, our results shed new light on the importance of denitrification in sedimentary diagenesis in the deepest part of the Earth's ocean, and could have important implications for understanding the current state of biogeochemical cycles in the hadal zone.

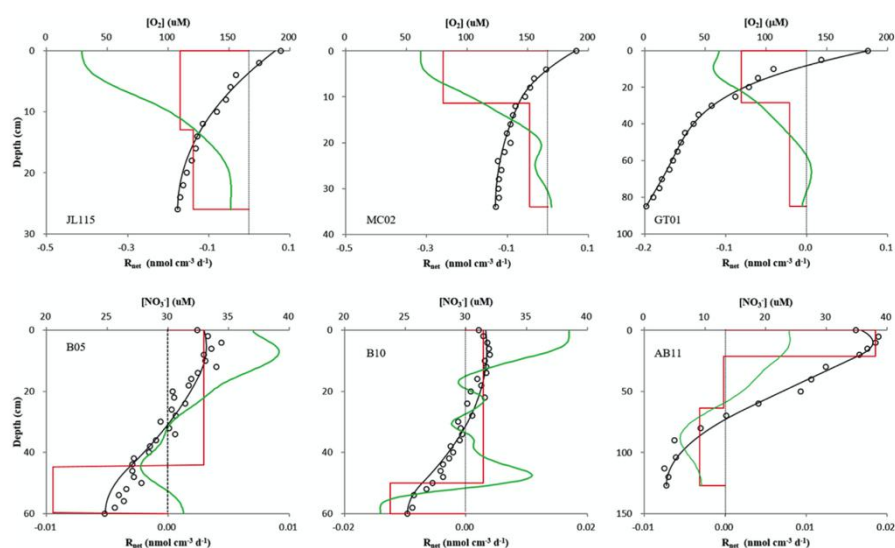


Fig1. Selected concentration profiles of DO and NO_3^- (blank dot) and the consumption rates as a function of depth (red step curves). The fits (blank lines) were obtained using the PROFILE interpretation software. The green solid lines represent the REC model output. The positive values indicate solute production and negative values indicate solute consumption. (For interpretation of the references to colour in this figure legend, the reader is referred to the Web version of this article.)

8. 反转场的角度依赖性对非磁滞剩磁应用的影响

翻译人: 张伟杰 12031188@mail.sustech.edu.cn



Finn, David, and Robert Coe. *Consequences of switching field angular dependence for applications of anhysteretic remanent magnetization [J]. Physics of the Earth and Planetary Interiors, 2020, 305:106507.*

<https://doi.org/10.1016/j.pepi.2020.106507>

摘要: 测量非磁滞剩磁(ARM)是评价许多重要岩石性质的一种简单的无损方法。ARM 包括应用一个交变磁场(AF)和一个直流偏置磁场(DF)来磁化岩石样品。ARM 的各种技术在解决构造、火山学、沉积学、环境和古气候以及更好地理解地磁场行为方面都取得了显著的成功。翻转场的角度依赖性对分析实际携带 ARM 的磁性颗粒的矫顽力和角度分布有重要的影响,然而,翻转场的角度依赖性往往没有引起足够的重视。结果普通的 ARM 测量方法并不能很好地达到预期的目的。例如,通过 ARM 逐步获得结果的微分或者 pARM(只在窄的 AF 窗口内打开直流场)不能够分离出特定矫顽力组分对 ARM 的贡献。测量目标矫顽力组分的 ARM 的最佳方法是微分峰值 AF 足够激活全部目标矫顽力区间所有的磁性矿物获得的 ARM 的逐步旋转退磁得到的结果。忽略活化的性质会导致高估相对古强度,低估高矫顽力颗粒浓度,放大 ARM 各向异性(如:自然剩磁校正中的误差),以及不同矫顽力组分的各向异性组构不必要的混合。

ABSTRACT: The measurement of anhysteretic remanent magnetization (ARM) is an easy nondestructive means of evaluating many important rock properties. This involves applying an alternating magnetic field (AF) along with a direct biasing field (DF) to magnetize rock samples. Various techniques employing ARM have been widely used with notable success to help solve problems in tectonics, volcanology, sedimentology, environmental and paleoclimate studies and to better understand geomagnetic field behavior. Often, however, too little attention is paid to the effects of switching field angular dependence, which has important influence on the coercivity and angular distributions of grains that actually carry the ARM. As a result, commonplace methods

of ARM measurement are not ideally designed for their intended purposes. For example, differentiation of a progressive ARM acquisition or turning on the direct field within a narrow AF window (i.e. partial ARM) are unable to isolate the ARM contribution from a specified coercivity grain fraction. Instead, the optimal method of measuring ARM in a targeted coercivity grain fraction is to differentiate a progressive tumble demagnetization of a total ARM generated with a peak AF high enough to fully activate the coercivity range of interest. Ignoring the activation property can lead to overestimation of relative paleointensity, underestimation of high coercivity grain concentrations, amplification of ARM anisotropy (e.g. error in natural remanence corrections), and unwanted mixing of anisotropy fabric components held in separate coercivity grain fractions.

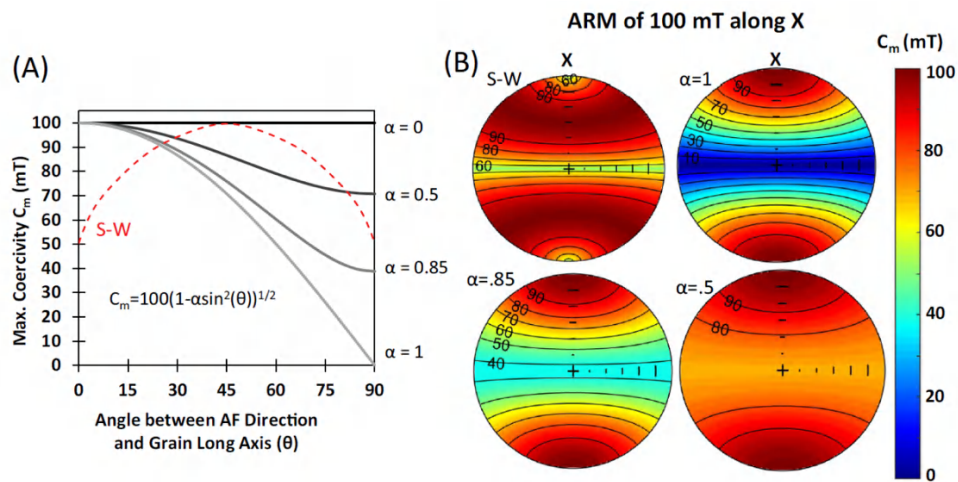


Fig1. Switching field angular dependence (Eq. (1b)) for a 100 mT ARM (A) as a function of angle θ between AF and grain long axis. The curves of C_m represent the highest coercivity activated (i.e., switched) for various angular dependence parameters (α). (The dependence for the Stoner-Wohlfarth (S-W) criterion is also shown for comparison). The contribution of unfavorably oriented (large θ) grains to the ARM becomes increasingly limited to lower coercivity grains with increasing switching field dependence. Note also that the coercivity range of fully activated grains, where all orientations contribute to the ARM, depends strongly on α ; e.g., for $\alpha = 0.85$, grains with coercivity from 0 to ~39 mT are fully activated, whereas those from 39 to 100 mT are only partially activated. (B) Equal area plots show this relationship in three dimensions

for the same ARM applied along the X axis. Each numbered contour is the maximum coercivity of grains with a particular orientation θ that carry the ARM.

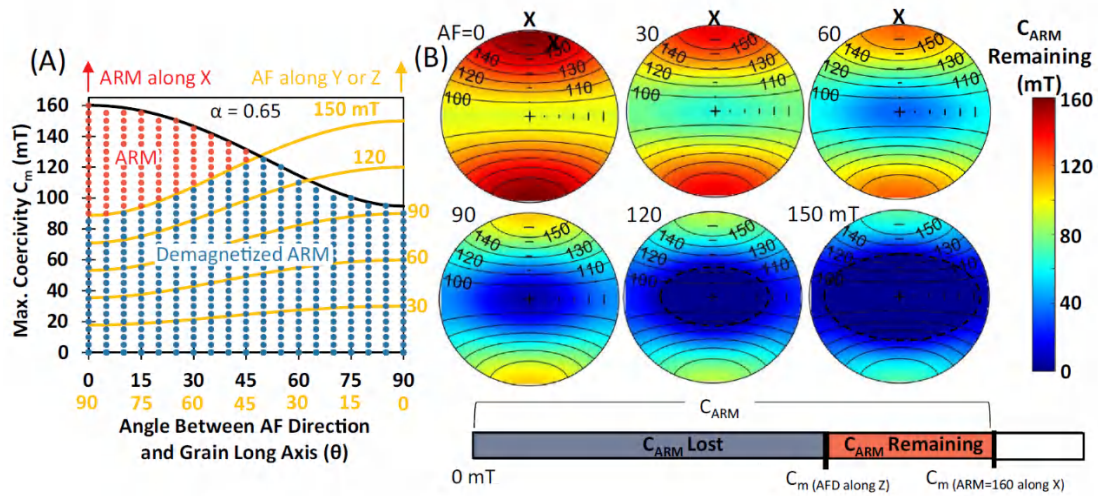


Fig2. Progressive 1-axis AF demagnetization applied orthogonal to a 160 mT ARM carried by grains that switch according to Eqs. (1a) and (1b) with angular dependence $\alpha = 0.65$. Low coercivity, unfavorably oriented grains that carry the ARM are first to go. (A) Two-dimensional rendering: blue stippled areas below yellow curves indicate orientations and coercivities of grains for which ARM is demagnetized by AFs of 30, 60, 90, 120 and 150 mT. Red stippled area indicates orientations and coercivities of grains for which ARM remains after demagnetization at 150 mT. Grains demagnetized at >95 mT were only partially activated by the ARM, whereas those <95 mT were fully activated. (B) Three-dimensional rendering: the labeled contours show the maximum coercivity of grains carrying an ARM (i.e. C_m) imparted along the sample's X direction with a peak AF of 160 mT. Color shading shows the range of coercivities carrying the ARM (C_{arm}). For example, the C_{arm} along X is around 70 mT after an ARM of 160 mT is imparted along X and a 150 mT demagnetizing AF is applied along Z (i.e. 160 mT \sim 90 mT). The dark blue, asymmetric angular windows indicated with a dashed black line encloses orientations for which all grains get demagnetized by 120 or 150 mT AF ($C_{arm} = 0$). This same region is indicated in Fig. 2A where the demagnetization (yellow) line exceeds that of the ARM (black). (For interpretation of the references to color in this figure legend, the reader is referred to the web version of this article.)

9. 死海沉积物记录地磁场长期变化信息

翻译人: 李海 12031330@mail.sustech.edu.cn



Ebert, Y, Shaar, R, & Stein, M. *Decadal geomagnetic secular variations from greigite bearing Dead Sea sediments*[J]. *Geochemistry, Geophysics, Geosystems*, 2021, 22, e2021GC009665.

<https://doi.org/10.1029/2021GC009665>

摘要: 黎凡特地区的古地磁数据揭示了全新世期间地磁场发生了快速的变化。然而可用的古地磁学数据较为零散,并且与区域的沉积记录的相关性较差。为了进一步探究地磁场方向的变化,作者研究了三个位于死海西部的晚全新世剖面。沉积物中的磁性特征受沉积环境的影响。靠近 EinGedi Spa 剖面的南部地区以碎屑钛磁铁矿为主, Nahal Og 和 Ein-Feshkha 剖面等北部地区则以自生胶黄铁矿为主。利用放射性碳测年建立剖面的年代框架。EF 剖面沉积物的主要载磁矿物为胶黄铁矿,记录了 2500 cal yr BP ~ 1000 cal yr BP 间可靠的地磁场信息。沉积物中的胶黄铁矿在沉积的早期便形成,因此平滑作用和倾角变浅的影响可以忽略不计。新的数据显示, 2400 cal yr BP ~ 2200 cal yr BP 间的虚地磁极与 GAD 的最大偏差有 20°, 在一个世纪的时间里,倾角由 60° 快速降低至 35°。这表明黎凡特铁器时代地磁异常与高的地磁活动有关。

ABSTRACT: Archaeomagnetic data from the Levant revealed periods within the Holocene with fast and extreme changes in the geomagnetic field. Yet, the availability of the archaeomagnetic data is sporadic and the correlation with the available sedimentary records from the region is rather poor. To further explore decadal variations in the directions of the field, we investigate three outcrops of the late Holocene Dead Sea that are exposed along the western retreating shores of the modern lake. The sediments were deposited under spatially varying limnological-environmental conditions, influencing their magnetic properties. The southern section, located near Ein-Gedi Spa (EG section) is dominated by detrital titanomagnetite whereas the northern sections - Nahal Og (Og section) and Ein-Feshkha (EF section) - are

dominated by authigenic greigite. The chronology of the sections was established by radiocarbon dating of short lived organic debris. The magnetic data were obtained in a 2cm resolution. The EF section, spanning the time interval from ca. 2500 cal yr BP to ca. 1000 cal yr BP, is dominated by greigite and thus providing the most robust geomagnetic record with precise paleomagnetic directions. Greigite forms very early in the sediment and the effects of smoothing and the inclination shallowing are negligible. The new data reveal a maximal deviation of 20° from the geocentric axial dipole field between 2400 to 2200 cal yr BP accompanied with a fast swing in inclination from 60° to 35° over about a century. This suggests high geomagnetic field activity associated with the Levantine Iron Age geomagnetic anomaly.

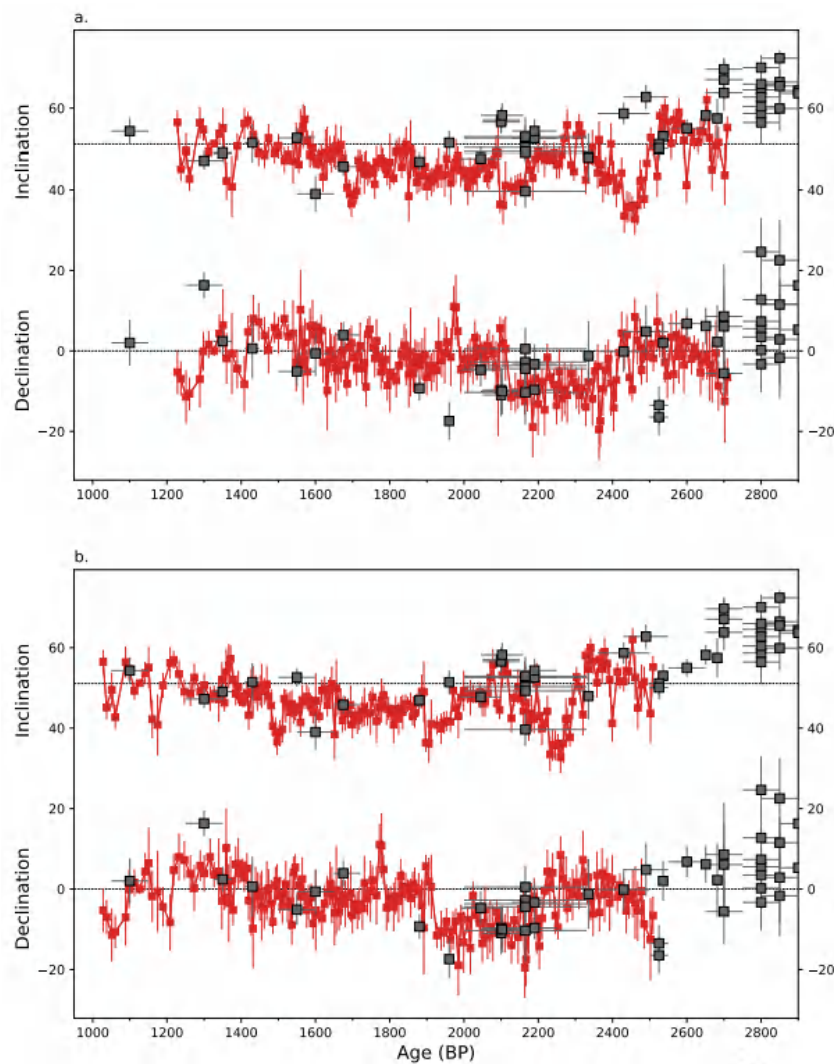


Fig1. Comparison between sedimentary and archaeomagnetic data. Mean directions of

the horizons in Ein-Feshkha are shown in red; archaeomagnetic data (Shaar et al., 2018; Tema et al., 2018; Tema et al., 2021) are shown in gray. Gray dashed lines represent the expected GAD directions. (a) EF data are plotted according to the depth-age model in Fig. 7. There are some dissimilarities between the two data sets. (b) Compatibility between the sedimentary and the archaeomagnetic data achieved after a shift of 200 years towards younger ages.

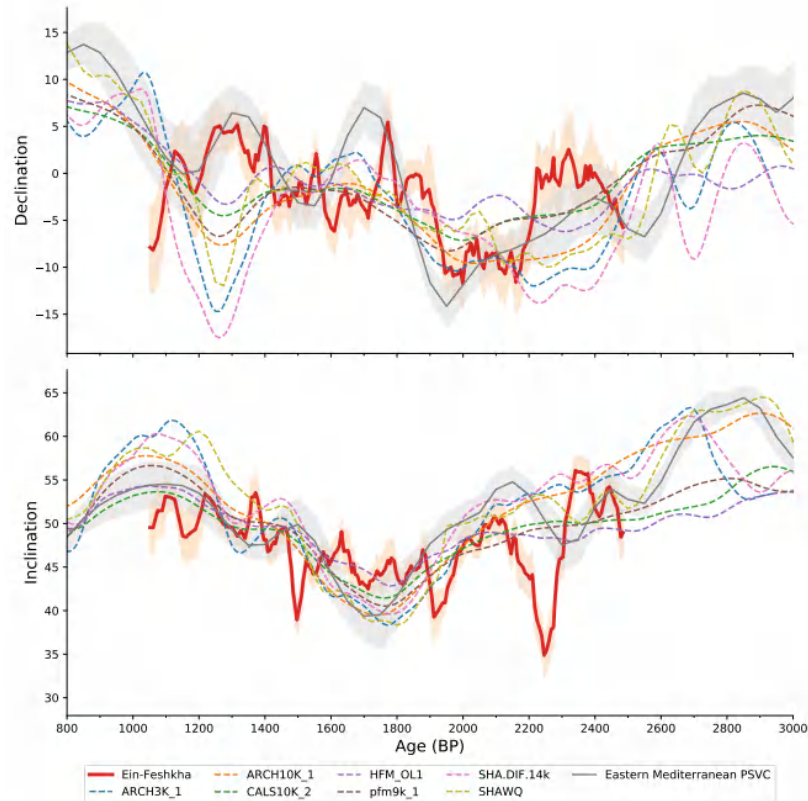


Fig2. Paleomagnetic data from Ein-Feshkha (EF) (red squares) plotted together with archaeomagnetic data (blue circles) from within a radius of ~600km around the Dead Sea. (a) Paleointensity data from Israel (Ben-Yosef et al., 2017; Shaar et al., 2011; Shaar et al., 2016; Vaknin et al., 2020), Jordan (Ben-Yosef et al., 2009), Syria (Gallet & Al-Maqdissi, 2010; Gallet et al., 2014; Gallet et al., 2006; Gallet et al., 2008; Genevey et al., 2003), and Cyprus (Shaar et al., 2015). (b-c) Declination and inclination from EF and from archaeomagnetism. Fast change in the inclinations of EF is observed between 2400 and 2200 cal yr BP (d) Deviation from the GAD; a deviation of 20° appears in EF at ~ 2200 yr BP suggesting a later decaying of the LIAA.

10. 多指标方法揭示南大西洋西部晚更新世沉积通量和底层水环境

翻译人: 张亚南 zhangyn3@mail.sustech.edu.cn



G. L. Mathias, S. C. Round, C. M. Chiessi, et al., A Multi-Proxy Approach to Unravel Late Pleistocene Sediment Flux and Bottom Water Conditions in the Western South Atlantic Ocean [J]. Paleoclimatology and Paleoclimatology, 2021, 36, 2020PA004058.

<https://doi.org/10.1029/2020PA004058>.

摘要: 沉积物中的磁学信号能够通过陆源磁性物质的供给来揭示过去大陆环境的变化, 但同时也通过原位形成的次生磁性矿物来记录过去的海洋环境信息。特别是在有其他独立指标来验证时。通过结合环境磁学、地球化学和硅质碎屑粒度数据, 作者对 GL-1090 钻孔 (24.92

°S, 42.51°W, 水深 2225m) 进行了研究, 揭示了近 184ka 南大西洋西部中深度区域陆源物质输入和底层水环境的变化。Al/Si, Fe/κ 和硅质碎屑粒度数据表明该钻孔的陆源沉积物来自于 Plata River (南美洲东南部)。这些物质通过巴西沿岸流向北输送到研究区域, 并受到海平面变化的影响。低海平面时期输入更多且较粗的陆源沉积物。环境磁学参数表明, 岩心钻孔在磁畴状态上具有明显的变化, 作者认为是冰期循环中生物成因磁铁矿含量的变化。磁性颗粒粒径和底栖 δ¹³C 的负偏表明, 单畴磁铁矿浓度 (可能是趋磁细菌磁铁矿) 反应了中深度水体通风的变化。作者认为, 冰盛期南大西洋西部中深度底层水通风的减弱导致了生物成因磁铁矿生成的减少。同时, 北大西洋深水停留时间的增加也反作用于冰盛期。

ABSTRACT: Magnetic signals in deep-sea sediments have the potential to unravel past continental environmental changes, via changes in primary terrigenous magnetic supply, but also record past marine environmental conditions, via in situ formation of secondary magnetic minerals, particularly when complemented by independent proxies. By combining environmental magnetic, geochemical, and siliciclastic grain size data, we investigated marine sediment core GL-1090 (24.92°S, 42.51°W, 2,225 m water depth) aiming to unravel changes in terrigenous sediment input and bottom water conditions during the last ~184 ka at the western South Atlantic middepth. The Al/Si, Fe/κ and

siliciclastic grain size data show that terrigenous sediments at this core location derived from the Plata River (southeastern South America). This material was transported northwards by the Brazilian Coastal Current and their delivery to our core site was modulated by sea-level oscillations. Periods of low sea-level were characterized by the input of coarser and more abundant terrigenous sediments. Environmagnetic parameters indicate significant downcore variations in the magnetic domain state, which we interpret as changes in the content of biogenic magnetite following glacial-interglacial cycles. Coeval negative excursions in magnetic grain size and benthic $\delta^{13}C$ suggests that concentrations of single domain magnetite (possibly magnetotactic bacterial magnetite) vary in response to middepth water ventilation. We suggest that reduced ventilation in the middepth western South Atlantic bottom waters during peak glaciations triggered a decrease in the production of biogenic magnetite. Peak glaciations were, in turn, linked with increases in the residence time of North Atlantic Deep Water (or its glacial counterpart).

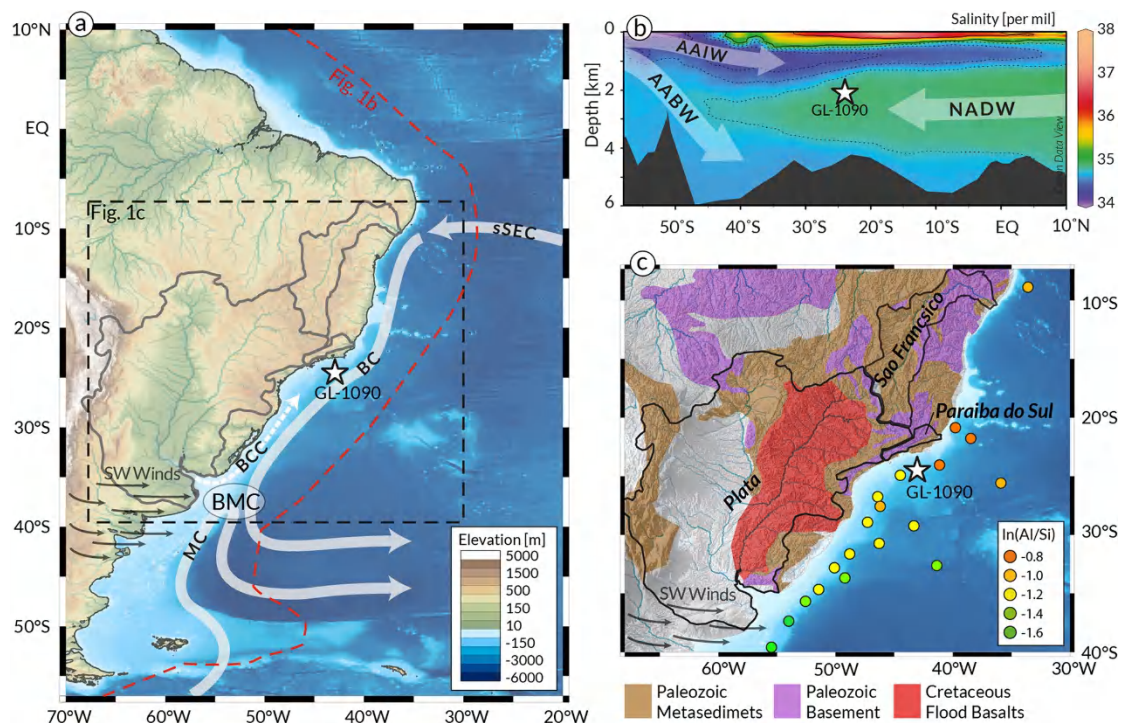


Fig1. Overview of the study area. The location of marine sediment core GL-1090 is shown in each panel by a white star. (a) Topographic map of South America with the

catchment area of rivers of interest that drain into the western South Atlantic outlined in black. The white arrows over the bathymetric map of the South Atlantic schematically depict the surface currents of interest (i.e., Brazilian Coastal Current [BCC], Brazil Current [BC] and Malvinas Current [MC]) as well as the Brazil - Malvinas Confluence (BMC). Thinner gray arrows show the Westerlies. The red and black dashed lines indicate the position of the salinity transect in Figure 1b and the location of Figure 1c, respectively. Topography and bathymetry from ETOPO1. (b) Western South Atlantic modern mean annual salinity. Main water masses are depicted by the gray arrows, Antarctic Intermediate Water (AAIW), North Atlantic Deep Water (NADW) and Antarctic Bottom Water (AABW). (c) Simplified geology of the major drainage basins, outlined in black, that represent relevant source areas for terrigenous material in the study area (geology simplified after/adapted from “World CGMW, 1:50M, Geologic Units Onshore” with sedimentary overburden removed) (Commission for the Geological Map of the World). Major tributaries of the Plata River are shown in blue. Colored dots on the adjacent continental margin indicate surface sediment in (Al/Si) values after Govin et al. (2012). This figure was partially produced using the software Ocean Data View.

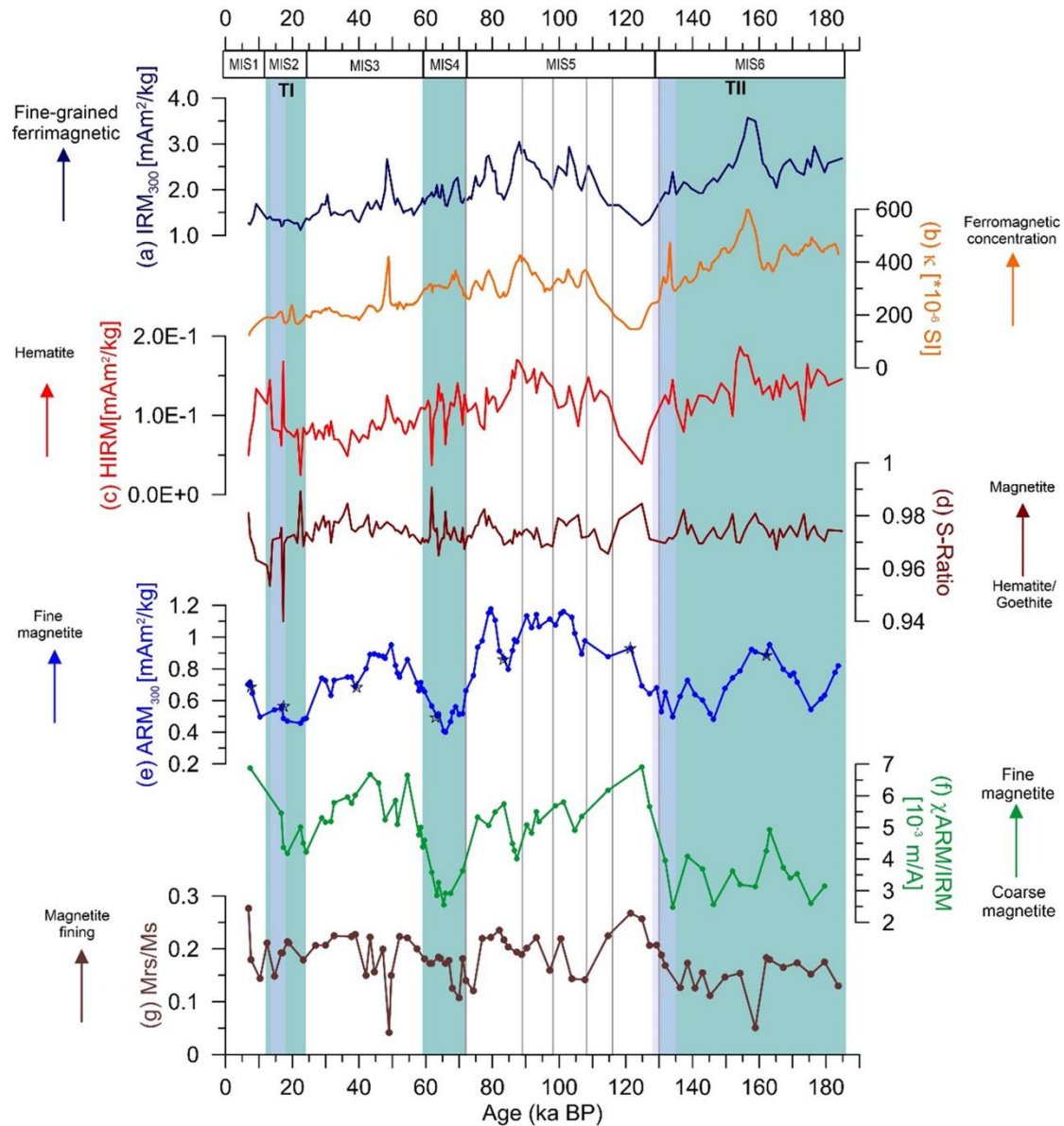


Fig2. Downcore environmental magnetic parameters (a)-(f), and hysteresis parameter Mrs/Ms (g) from marine sediment core GL-1090. (a) IRM300, (b) magnetic susceptibility (κ), and (c) HIRM, record changes in the concentration of magnetic minerals. (d) S-Ratio, records relative changes in magnetite versus haematite. (e) ARM300 reflects changes in the concentration of fine magnetic grains, (f) χ_{ARM}/IRM , and (g) Mrs/Ms record changes in the relative proportion of fine magnetite vs. course magnetite. Black stars in plot (e) show the samples we performed FORC analysis. The main lithological changes vary accordingly with cold/warm stages, blue/white bars, respectively, which represent marine isotope stages. Gray lines represent the MIS 5 stages, and gray bars show Terminations II and I.

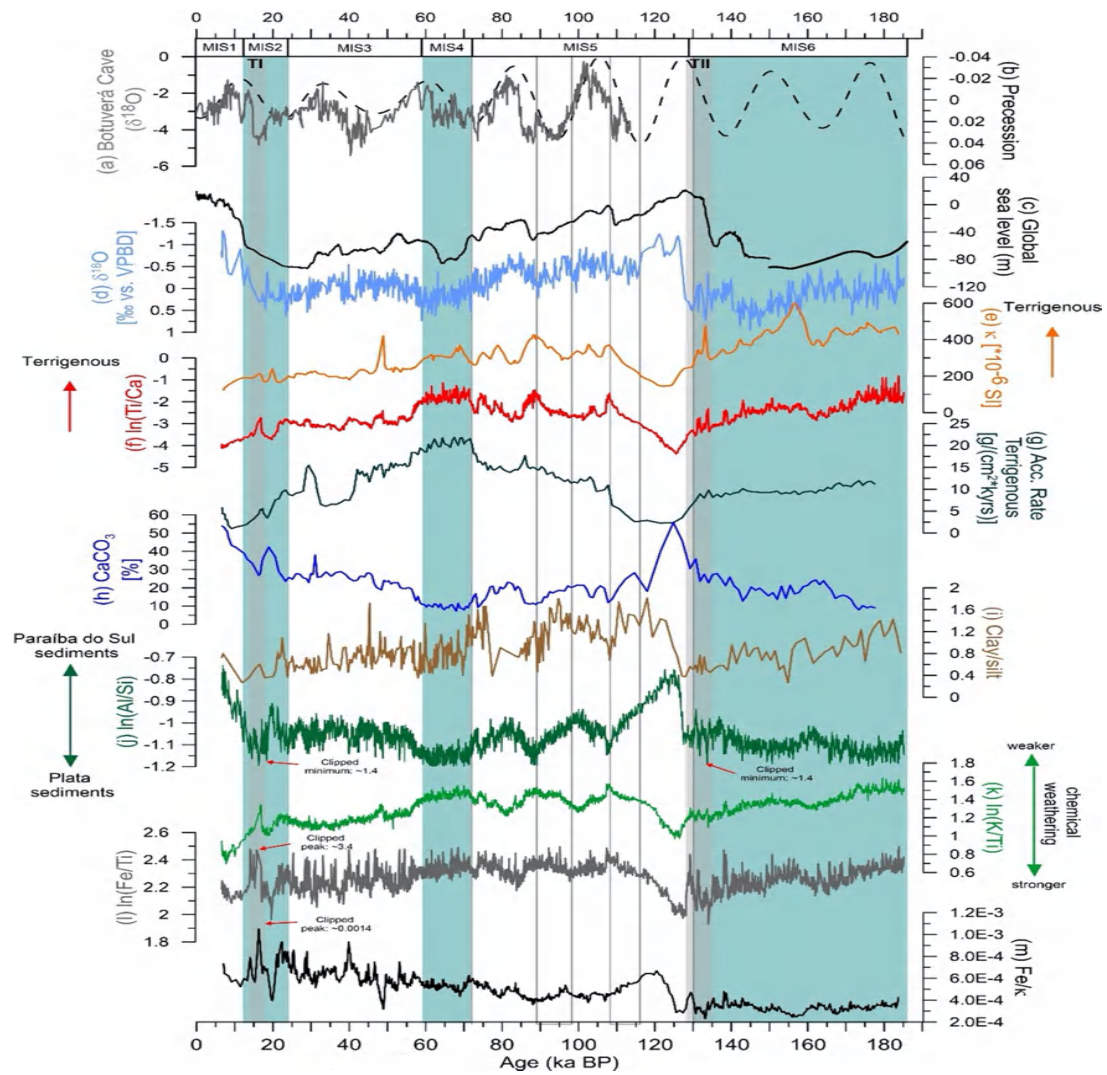


Fig3. Downcore parameters from marine sediment core GL-1090. External literature: (a) Speleothem $\delta^{18}\text{O}$ from Botuverá Cave, (b) Precession, (c) Global Sea Level for the last 150 and between 150 and 186 ka, (d) *Globigerinoides ruber* $\delta^{18}\text{O}$, and (h) CaCO_3 (%); parameters for sediment provenance: (e) magnetic susceptibility, (f) Ti/Ca, (g) accumulation rate of terrigenous, (i) Clay/Silt, (j) Al/Si, (k) K/Ti, and reductive proxies: (l) Fe/Ti and (m) Fe/ κ . The main lithological changes vary accordingly with cold/warm stages, blue/white bars, respectively, which represent marine isotope stages. Gray lines represent the MIS 5 stages, and gray bars show Terminations II and I.